JOC The Journal of Organic Chemistry

Featured Article

Cite This: J. Org. Chem. 2019, 84, 12253−12258

pubs.acs.org/joc

Axial Chirality at the Boron−Carbon Bond: Synthesis, Stereodynamic Analysis, and Atropisomeric Resolution of 6-Aryl-5,6-dihydrodibenzo[*c*,*e*][1,2]azaborinines

Andrea Mazzanti, Maria Boffa, Emanuela Marotta, and Michele Mancinelli*

Department of Industrial Chemistry "Toso Montanari", University of Bologna, Viale del Risorgimento 4, Bologna 40136, Italy

Supporting Information

ABSTRACT: 6-Aryl-5,6-dihydrodibenzo[*c*,*e*][1,2]azaborinines display restricted rotation at the boron−carbon aryl bond, yielding conformational isomers or atropisomers. The stereodynamic processes were monitored by variable-temperature NMR (D-NMR), dynamic enantioselective HPLC (D-HPLC), or kinetic racemization measurements. The absolute configuration of stable atropisomers (compound **1d**, $\Delta G^{\ddagger}_{rac}$ = 26.0 kcal·mol^{-1}) was determined by TD-DFT simulation of the electronic circular dichroism (ECD) spectra. The racemization energy of **1d** is more than 12 kcal·mol^{-1} smaller than its isostere 9-(2-methylnaphthalen-1-yl)phenanthrene.

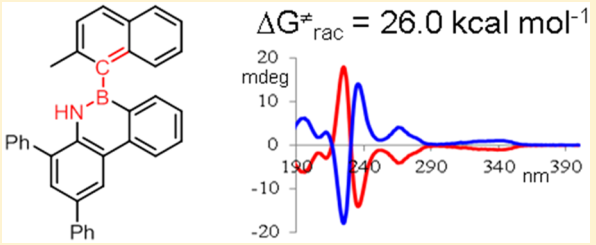

INTRODUCTION

Azaborines are part of a class of chemical compounds that has emerged in the recent past, affecting many research fields.[1] The azaborine moiety replaces a C=C bond with a B−N bond within any molecular structure to obtain isosteric and isoelectronic architectures. The polarity of the B−N bond imparts different chemical and physical properties to the molecular structure. Due to the large electronegativity difference, π electrons are mainly shifted toward the nitrogen, leading to slightly less aromatic and less stable compounds. The inclusion of heteroatoms and π-conjugated fragments is a strategy that allows us to find new materials with unique functions because the presence of the unbalanced electron distribution changes the electronic and photophysical properties of potential organic semiconductors. The replacement of one or more of the carbon atoms in polycyclic aromatic hydrocarbons (PAHs) with boron decreases the HOMO−LUMO gap, providing an access to molecules with chemiluminescent properties. Azaborines have been shown to be effective organic light-emitting diodes (OLEDs)[2] and organic field-effect transistors (OFETs).[3] Moreover, these types of organic compounds are important for the design of additional structures with biological functions for the research of new drugs candidates.[4] The latter concept is very interesting because the trivalent structure of the boron can give alternative electrostatic contacts with the enzymatic targets. Recently, 2-aryl-2,1-borazaronaphthalenes (i.e., the isosters of a 2-aryl-1-naphthalenes compounds) have been shown to yield atropisomeric structures, configurationally stable at ambient temperature.[5] Following this previous work, we have analyzed the boron−carbon stereogenic axis in the analogues of 9-arylphenanthrene (and 1-arylnaphthalenes as well) and 6-aryl-5,6-dihydrodibenzo[*c*,*e*][1,2]azaborinines (**1a**−**1d** in Scheme 1), where the B−N moiety has been reversed in geometry with respect to the previous compounds.

Scheme 1. Compounds 1a−1d

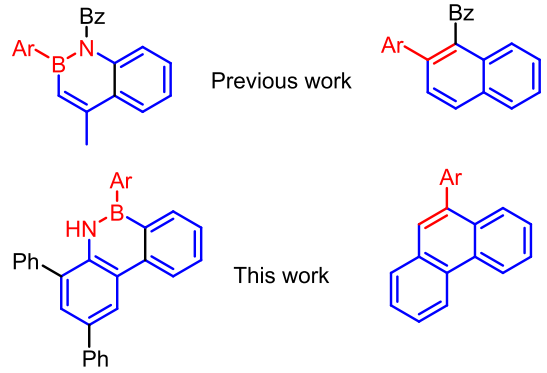

RESULTS AND DISCUSSION

As in the paradigmatic case of biphenyls,[6] when an unsymmetrically *ortho*-substituted aryl ring is bound to the boron in compounds **1a**−**1d** (Scheme 1), it is skewed out of the plane because of the steric hindrance between the *ortho* substituent and the NH and CH in positions 5 and 7, thus implying the formation of two enantiomeric conformations.

Received: June 11, 2019
Published: July 19, 2019

DOI: 10.1021/acs.joc.9b01550
J. Org. Chem. 2019, 84, 12253−12258

The thermal stability of these conformational enantiomers relies on the steric hindrance of the *ortho* substituent[7] and the peculiar features of the carbon−boron bond, as this was found to be significantly longer than a carbon−carbon bond (1.58 vs 1.49 Å).[5]

DFT calculations were preliminary run on compound **1a** (Ar = *o*-tolyl) using B3LYP[8] and the 6-31G(d) basis set. The optimized geometries (see Figure 1) suggest that in the two

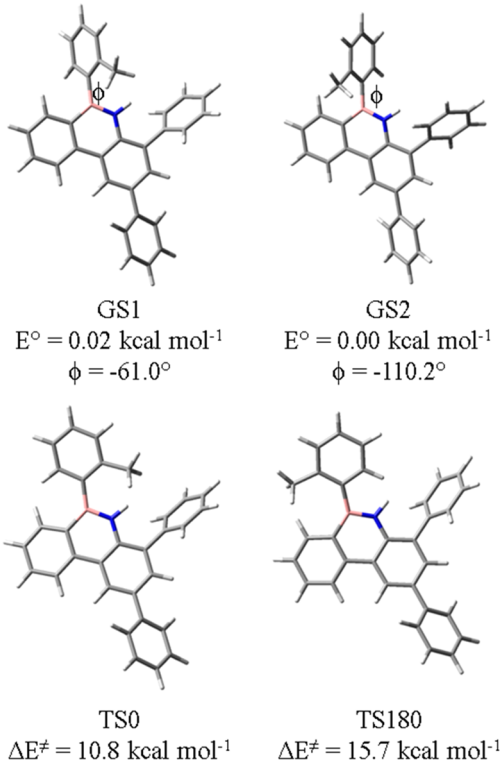

Figure 1. Ground and transition states for compound **1a** (only the *M* atropisomer is shown, relative energies in kcal·mol^{-1}).

skewed conformations[6b] the *o*-tolyl ring is displaced out of the plane by |61|° or by |110|° (N−B−C_q−C_{ortho} dihedral angle, ϕ in Figure 1), with a C−B bond length of 1.58 Å. The threshold transition state for the interconversion of the atropisomeric pair was calculated as 10.8 kcal·mol^{-1}, and it corresponds to the rotation of the *o*-methyl over the NH (TS0 in Figure 1). This rotational barrier should be easily monitored by the dynamic NMR (D-NMR) technique in the presence of a chirality probe, such as the ethyl group in compound **1b**.

Compounds **1a−1d** were prepared by modifying a synthetic procedure that has been recently reported.[9] The key step of the synthesis is a Friedel−Crafts reaction that yields the intermediate **2**, using BCl_3 and $AlCl_3$ (Scheme 2).[10] The use of different nucleophilic aryl groups, e.g. Grignard reagents, allowed the synthesis of compounds **1a−1d**.

It has been reported that the use of a glovebox was mandatory because of the sensitivity of intermediate **2** to air and moisture. To make the preparation available to standard laboratory equipment, we have modified this procedure to be performed in "one pot" by generating in situ both intermediate **2** and the Grignard reagent. The synthetic procedure was optimized on product **1a** (see the Experimental section), but this compound was unsuitable for the NMR determination of the C−B rotational barrier because of the absence of any

Scheme 2. Synthesis of Compounds 1a−1d

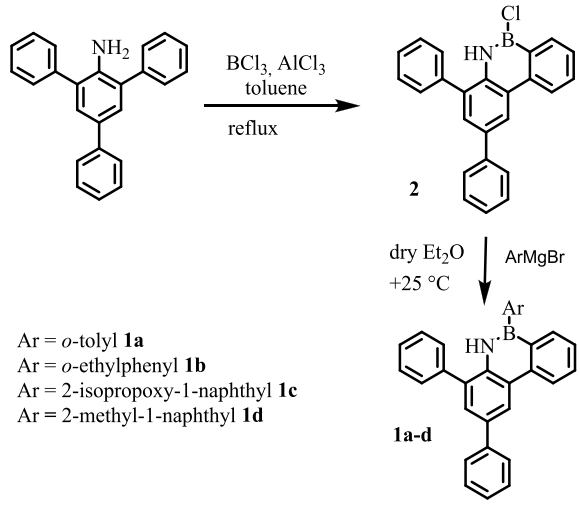

chirality probe.[11] Compound **1b**, bearing an *o*-ethylphenyl group as probe of chirality, was prepared and analyzed by means of D-NMR spectroscopy (Figure 2, left). At ambient temperature the signal of the CH_2 was a quartet, thus implying fast rotation in the NMR time scale. On lowering the temperature, the signal reached the coalescence point at −15 °C and eventually split into two signals below −40 °C (ABX_3 spin system). Line shape simulation allowed us to determine the rate constants for the dynamic process at the different

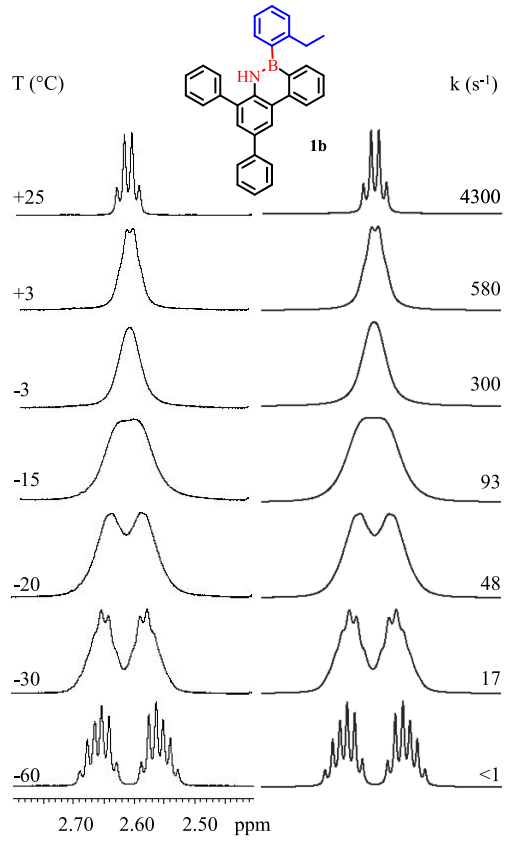

Figure 2. (Left) Variable-temperature NMR spectra of the CH_2 signal of compound **1b** (600 MHz in CD_2Cl_2). (Right) Line-shape simulation of the ABX_3 system with the corresponding rate constants.

DOI: 10.1021/acs.joc.9b01550
J. Org. Chem. 2019, 84, 12253−12258

temperatures, hence, the activation free energy (12.6 ± 0.15 kcal·mol^{-1}) by means of the Eyring equation (Table 1). The

Table 1. Experimental and Calculated Free Energy Barriers (kcal·mol^{-1})

compd	$\Delta G^{\ddagger}_{calc}$	$\Delta G^{\ddagger}_{exp}$
1a	10.8	not determinable
1b	13.2	12.6 (D-NMR, −30 to +3 °C)
1c	21.5	21.8 (D-HPLC, +15 to +45 °C)
1d	25.3	26.0 (kinetic racemization, +45 and +50 °C)
3	38.0	>38.1 (+146.5 °C)

experimental value is well reproduced by DFT calculations performed on compound **1a**, taking into account the slightly larger steric hindrance of the ethyl group with respect to methyl (B = 7.4 kcal·mol^{-1} for Me and 8.7 kcal·mol^{-1} for Et).[7]

Compound **1c** has a higher steric hindrance with respect to **1b** due to the presence of the 2-isopropoxy-1-naphthyl group. D NMR analysis showed there was no exchange between the two diastereotopic CH_3 signals of isopropyl up to +120 °C. When analyzed on chiral stationary phase HPLC (CSP-HPLC) at +25 °C, compound **1c** showed two resolved chromatographic peaks for the two atropisomers, but the presence of a plateau between the peaks suggested that on-column racemization took place.[12] The chromatographic runs were then recorded within +15 and +45 °C (continuous cyan lines in Figure 3), and the kinetic rate constants were evaluated through line-shape simulation of the chromatograms[13] (dashed

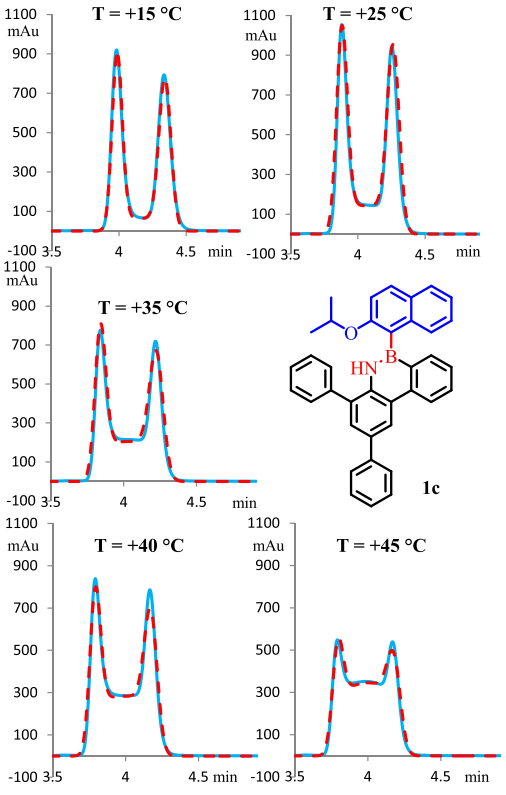

Figure 3. D-HPLC chromatograms for compound **1c** on CSP column (cyan lines, ChiralPak AD-H 250 × 4.6 mm, *n*-hexane/2-propanol 95:5 v/v, 1 mL·min^{-1}). Red dashed lines are the simulated chromatograms.

red lines in Figure 3). The $\Delta G^{\ddagger}$ derived by Eyring equation was 21.8 ± 0.2 kcal·mol^{-1} (Figure S4), corresponding to a lifetime of ≈1000 s at +25 °C.[14]

Compound **1d** was therefore prepared to further increase the steric hindrance and to obtain thermally stable atropisomers. In this case, the CSP-HPLC analysis showed two well-separated peaks (Figure 4, top), and a semi-

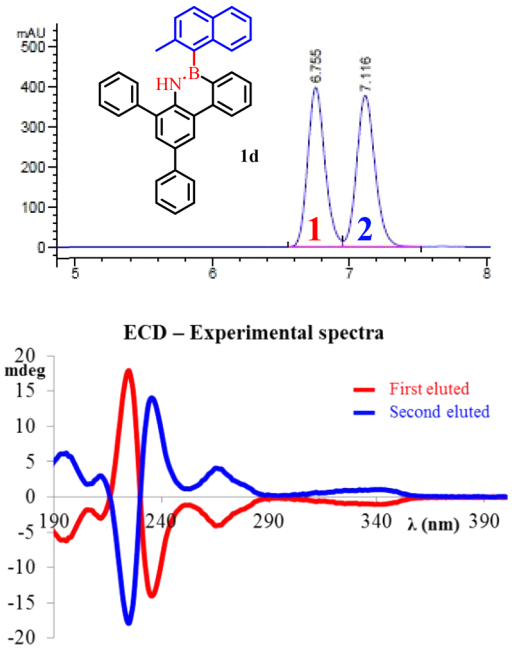

Figure 4. (Top) CSP-HPLC chromatogram of compound **1d** (ChiralPak AD-H 250 × 4.6 mm, *n*-hexane/2-propanol 97:3, 1 mL·min^{-1}). (Bottom) ECD spectra of the two atropisomers (in CH_3CN).

preparative approach allowed us to resolve the two atropisomers and to record their ECD spectra (Figure 4, bottom). The racemization rate was derived by kinetic analysis at +45 and +50 °C (Figure S5). A sample of enantiopure atropisomer was heated, and the racemization process was followed by analytical CSP-HPLC (Figure S5). A racemization barrier of 26.0 ± 0.2 kcal·mol^{-1} (DFT-calculated value was 25.3 kcal·mol^{-1}) was derived from the rate constants determined at the two different temperatures, corresponding to a half-life time of 30 days at +25 °C. This value has to be compared with that of the isoster 9-(2-methylnaphthalen-1-yl)phenanthrene (**3**, $\Delta G^{\ddagger}_{rac}$ > 38 kcal·mol^{-1}, see SI for details), yielding a $\Delta\Delta G^{\ddagger}$ > 12 kcal·mol^{-1}. This large difference is a direct consequence of the longer C−B bond with respect to C−C.

The absolute configuration of the two atropisomers of **1d** was assigned by the simulation of ECD spectrum based on time-dependent density functional theory (TD-DFT).[15] A conformational search suggested the existence of four conformations, with very similar energies, due to the different dihedral angles of the two phenyl rings in positions 2 and 4 (Figure S3). The theoretical ECD spectra of the four ground-state conformations (Figure 5) were obtained with four different functionals (CAM-B3LYP,[16] ωB97X-D,[17] BH&HLYP,[18] and M06-2x[19]) with the same 6-311++G(2d,p) basis set in order to have data redundancy and to enhance reliability. The spectra simulated for the four conformations have similar shapes, with a negative band between 220 and 250

DOI: 10.1021/acs.joc.9b01550
J. Org. Chem. 2019, 84, 12253−12258

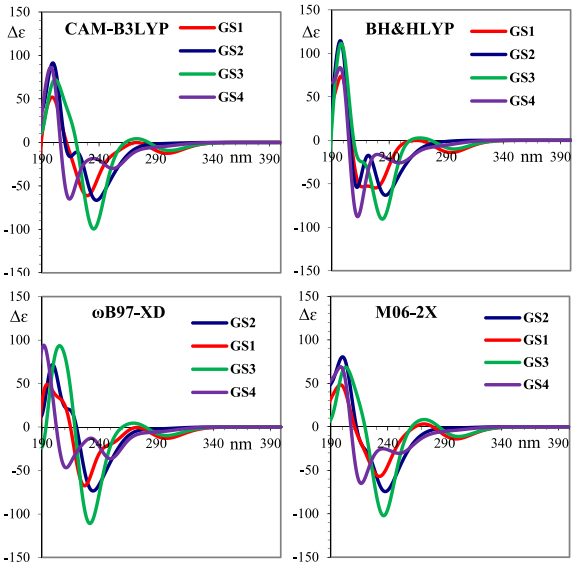

Figure 5. Computed spectra for the four conformations of the *M* atropisomer of compound **1d**. Calculations were obtained using the same 6-311++G(2d,p) basis set.

nm and one positive between 190 and 210 nm. As a consequence, the Boltzmann-averaged ECD spectrum is not very sensitive to variations of the conformational ratio.

The conformationally averaged spectra, obtained using the ZPE-corrected enthalpies suggested by B3LYP/6-31G(d) optimization, are in good agreement with the experimental spectrum of the first eluted atropisomer, to which the *M* absolute configuration can be assigned (Figure 6).

In summary, we have shown that 6-aryl-5,6-dihydrodibenzo-[*c*,*e*][1,2]azaborinines yield configurationally stable atropisomers when bearing an hindered *ortho*-substituted aryl ring such as 2-methylnaphthalene. However, the racemization energy of compound **1d** is more than 12 kcal·mol^{-1} smaller that its isoster 9-(2-methylnaphthalen-1-yl)phenanthrene **3**.

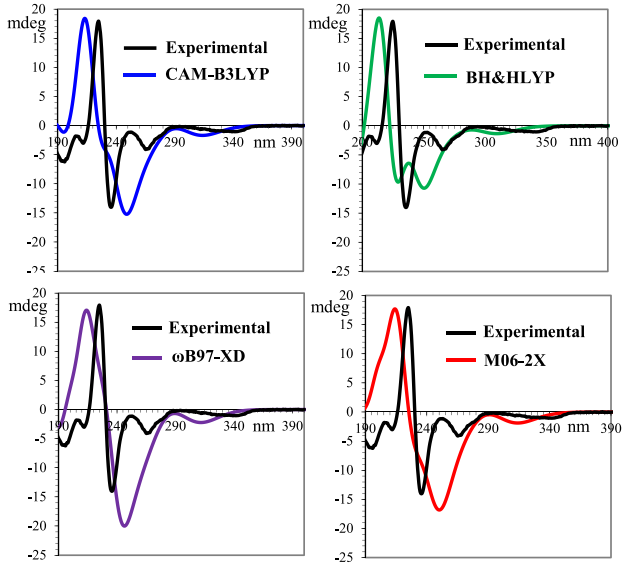

Figure 6. Experimental and calculated ECD of **1d**. The spectra calculated for the *M* atropisomer have been red-shifted by 14, 16, 15, and 14 nm and multiplied by a scale factor of 0.25, 0.19, 0.31, and 0.27 for CAM-B3LYP, BH&HLYP, ωB97X-D, and M06-2x, respectively. The experimental spectrum (black) is that of the first eluted atropisomer (Figure 4).

EXPERIMENTAL SECTION

NMR Spectroscopic data. NMR spectra were recorded using a spectrometer operating at a field of 14.4 T (600 MHz for ^{1}H, 150.8 for ^{13}C, 192.4 for ^{11}B). Chemical shifts are reported in ppm (δ) relative to TMS as an internal standard. The 150.8 MHz ^{13}C spectra were acquired under proton-decoupling conditions with a 36000 Hz spectral width, 5.5 μs (60° tip angle) pulse width, 1 s acquisition time, and 9 s delay time. The long relaxation time was needed to observe some quaternary carbons. A line broadening function of 1−2 Hz was applied before the Fourier transformation. ^{13}C signals were assigned by DEPT-135 sequence. Variable-temperature NMR spectra were recorded as previously reported.[20] The rate constants were derived from line shape simulations (QCPE DNMR6 program),[21] and the free energies of activation ($\Delta G^{\ddagger}$) were obtained by means of the Eyring equation. Within the experimental uncertainty, the latter values were found to be essentially invariant in the examined temperature range, thus implying an almost negligible activation entropy $\Delta S^{\ddagger}$. HRMS were performed with an ESI-QTOF spectrometer at the CIGS facility, Modena, Italy.

Calculations. The ground-state and transition-state geometries were obtained using the Gaussian 16 rev A.03 series of programs,[22] with standard optimization parameters. The calculations employed the B3LYP hybrid-DFT functional[8] and the 6-31G(d) basis set. Vibrational analysis was performed to validate the ground states (zero imaginary frequencies) and the transition states (one imaginary frequency). Visual inspection of the corresponding normal mode[23] confirmed the identification of the correct transition states. Where not explicitly indicated, the reported energies are uncorrected electronic energies. TD-DFT calculations were performed by means of the hybrid functionals BH&HLYP[18] and M06-2x,[19] the long-range correlated ωB97X-D that includes empirical dispersion,[17] and CAM-B3LYP that includes long-range correction using the Coulomb Attenuating Method.[16] The 6-311++G(2d,p) was used for all of the TD-DFT calculations. For each simulation, 70 transitions were calculated, and the spectra were obtained by applying Gaussian shapes (half line width at half height = 0.25 eV). The Boltzmann-averaged UV spectrum was red-shifted in order to match the experimental UV spectrum (see the SI), and the same correction was applied to the simulated ECD spectra. A vertical scale factor was used in order to match the intensity of the most intense band of the experimental ECD spectrum.

ECD Spectra were recorded at +25 °C in far-UV HPLC-grade acetonitrile solutions. The concentrations of the samples (about 10^{-4} M) were tuned by dilution of a mother solution to obtain a maximum absorbance of about 0.8−1.0 in the UV spectrum using a 0.2 cm path length. The ECD spectra were recorded in the 190−400 nm interval as the average of 16 spectra.

Materials. 2,4,6-Triphenylaniline, 2-bromo-1-naphthol, 2-methyl-1-bromonaphthalene, and 2-ethyl-1-bromobenzene were commercially available and were used as received. 9-(2-Methylnaphthalen-1-yl)phenanthrene (**3**) was prepared according to the literature.[24]

General Procedure for the Preparation of 6-Aryl-5,6-dihydrodibenzo[*c*,*e*][1,2]azaborinines 1a−1d. Preparation of compounds **1a−1d** was carried out in a two-necked flask under nitrogen atmosphere. The reflux condenser was fitted with a drying tube packed with calcium chloride. To a dry toluene solution (20 mL) of 2,4,6-triphenylaniline (0.500 g, 1.56 mmol) was added BCl_3 (4.7 mL, 1 M solution in *n*-hexane, 3 equiv) dropwise at 0 °C. A precipitate formed when the BCl_3 solution was added, but it gradually dissolved, and the reaction mixture became clear again. It was then heated to reflux for 30 min under stirring and cooled again to ambient temperature. Thereafter, a catalytic amount of $AlCl_3$ (2 mol %) was added, and the reaction mixture was refluxed again for 18 h to obtain compound **2**. The crude was dried under vacuum to remove the

DOI: 10.1021/acs.joc.9b01550
J. Org. Chem. 2019, 84, 12253−12258

solvent, any traces of water, and volatile components such as hydrogen chloride and boron chloride. The green solid obtained after evaporation was dissolved by addition of dry Et_2O (24 mL). A solution of the appropriate Grignard reagent (4 mL, 0.5 M in Et_2O, freshly prepared in another two-necked flask) was then added to intermediate **2**. The resulting mixture was left under magnetic stirring for 1 h at ambient temperature. The reaction was quenched with H_2O and extracted with Et_2O (3 × 20 mL), and the organic layers were dried over $MgSO_4$. They were filtered first on a plug of silica gel and then on a plug of Celite with EtOAc as eluent. The crude compound was purified by chromatography on silica gel (petroleum ether/EtOAc 19:1). Analytically pure samples of compounds **1a−1d** were obtained by reversed-phase semipreparative HPLC with a Phenomenex Synergi Polar-RP 80 Å column (250 × 10 mm, ACN/H_2O 90:10 v/v).

2,4-Diphenyl-6-(o-tolyl)-5,6-dihydrodibenzo[c,e][1,2]azaborine ***1a***. Yield: 35% (230 mg). ^{1}H NMR (600 MHz, CD_2Cl_2, 5.33 ppm, +25 °C): δ 2.20 (s, 3H), 7.10 (t, J = 7.4 Hz, 1H), 7.14 (d, J = 7.5 Hz, 1H), 7.19 (td, J = 7.6, 1.6 Hz, 1H), 7.26−7.31 (m, 2H), 7.34 (tdd, J = 7.5, 1.8, 1.3 Hz, 1H), 7.37−7.50 (m, 5H), 7.46−7.50 (m, 2H), 7.59 (d, J = 2.1 Hz, 1H), 7.66−7.72 (m, 3H), 7.77 (dd J = 7.4, 1.2 Hz, 1H), 7.89 (bs, NH), 8.58 (d, J = 8.3 Hz, 1H), 8.66 (d, J = 2.1 Hz, 1H). ^{13}C{^{1}H} NMR (150.8 MHz, CD_2Cl_2, 53.52 ppm, +25 °C): δ 22.6 (CH_3), 121.8 (CH), 122.5 (CH), 123.9 (Cq), 124.7 (CH), 126.3 (CH), 127.0 (CH), 127.0 (CH), 128.1 (CH), 128.18 (CH), 128.3 (CH), 128.8 (CH), 129.3 (CH), 129.7 (CH), 131.2 (CH), 132.4 (Cq), 132.9 (CH), 134.1 (Cq), 135.3 (Cq), 136.5 (CH), 138.4 (Cq), 139.0 (Cq), 140.5 (Cq), 141.1 (Cq). ^{11}B NMR (192.4 MHz, $CDCl_3$, BF_3·Et_2O = 0 ppm, +25 °C): δ 38.13. HRMS (ESI-QTOF): calcd for $C_{31}H_{25}BN$ $[M + H]^+$ 422.2075, found 422.2071.

6-(2-Ethylphenyl)-2,4-diphenyl-5,6-dihydrodibenzo[c,e][1,2]-azaborine ***1b***. Yield: 32% (217 mg). ^{1}H NMR (600 MHz, CD_2Cl_2, 5.33 ppm, +25 °C): δ 1.05 (t, J = 7.6 Hz, 3H), 2.51 (q, J = 7.6 Hz, 2H), 7.11 (td, J = 7.2, 1.1 Hz, 1H), 7.19 (d, J = 7.6 Hz, 1H), 7.24 (td, J = 7.7, 1.2 Hz, 1H), 7.26−7.32 (m, 2H), 7.33−7.46 (m, 5H), 7.47−7.50 (m, 2H), 7.60 (d, J = 2.0 Hz, 1H), 7.68−7.72 (m, 2H), 7.74 (dd, J = 7.4, 0.9 Hz, 1H), 7.97 (bs, NH), 8.59 (d, J = 8.2 Hz, 1H), 8.67 (d, J = 1.9 Hz, 1H). ^{13}C{^{1}H} NMR (150.8 MHz, CD_2Cl_2, 53.52 ppm, + 25 °C): δ 16.4 (CH_3), 29.6 (CH_2), 121.9 (CH); 122.5 (CH), 124.1 (Cq), 124.9 (CH), 126.4 (CH), 127.1 (CH), 127.2 (CH), 127.8 (CH), 128.2 (CH), 128.4 (CH), 128.9 (CH), 129.4 (CH), 129.7 (CH), 131.3 (CH), 132.5 (Cq), 133.0 (CH), 134.2 (Cq), 135.4 (Cq), 136.7 (CH), 138.5 (Cq), 139.1 (Cq), 141.2 (Cq), 147.3 (Cq). ^{11}B NMR (192.4 MHz, $CDCl_3$, BF_3·Et_2O = 0 ppm, +25 °C): δ 38.33. HRMS (ESI-QTOF): calcd for $C_{32}H_{27}BN$ $[M + H]^+$ 436.2231, found 436.2233.

6-(7-Isopropoxynaphthalen-1-yl)-2,4-diphenyl-5,6-dihydrodibenzo[c,e][1,2]azaborinine ***1c***. Yield: 34% (273 mg). ^{1}H NMR (600 MHz, CD_2Cl_2, 5.33 ppm, +25 °C): δ 1.116 (d, J = 6.1 Hz, 3H), 1.122 (d, J = 6.1 Hz, 3H), 4.60 (sept, J = 6.1 Hz, 1H), 7.23 (qt, J = 6.8, 1.3 Hz, 1H), 7.30 (td, J = 6.8, 1.0 Hz, 1H), 7.35 (d, J = 9.1 Hz, 1H), 7.37−7.44 (m, 3H), 7.45−7.57 (m, 3H), 7.54 (t, J = 7.6 Hz, 2H), 7.62 (dd, J = 8.3, 1.2 Hz, 2H), 7.70 (dd, J = 6.9, 1.2 Hz, 1H), 7.74 (d, J = 1.9 Hz, 1H), 7.79−7.86 (m, 4H), 7.9 (d, J = 9.0 Hz, 1H), 8.29 (bs, NH), 8.74 (d, J = 8.3 Hz, 1H), 8.84 (d, J = 1.9 Hz, 1H). ^{13}C{^{1}H} NMR (150.8 MHz, $CDCl_3$, 77.36 ppm, +25 °C): δ 22.1 (CH_3), 22.2 (CH_3), 71.2 (CH), 116.4 (CH), 122.0 (CH), 122.5 (CH), 123.3 (CH), 124.2 (Cq), 125.7 (CH), 126.2 (CH), 127.1 (CH), 127.2 (CH), 128.06 (CH), 128.09 (CH), 128.4 (CH), 128.9 (CH), 129.2 (Cq), 129.3 (CH), 129.8 (CH), 130.1 (CH), 131.2 (CH), 132.4 (Cq), 135.8 (Cq), 136.8 (CH), 137.7 (Cq), 138.6 (Cq), 138.8 (Cq), 141.3 (Cq), 158.2 (Cq). 11B NMR (192.4 MHz, $CDCl_3$, BF_3·Et_2O = 0 ppm, +25 °C): δ 38.64. HRMS (ESI-QTOF): calcd for $C_{37}H_{31}BNO[M + H]^+$ 516.2493, found 516.2496.

6-(2-Methylnaphthalen-1-yl)-2,4-diphenyl-5,6-dihydrodibenzo-[c,e][1,2]azaborinine ***1d***. Yield: 36% (265 mg). ^{1}H NMR (600 MHz, CD_2Cl_2, 5.33 ppm, +25 °C): δ 2.39 (s, 3H), 7.27 (qd, J = 6.8, 1.2 Hz, 1H), 7.36−7.46 (m, 5H), 7.46−7.54 (m, 3H), 7.56 (t, J = 7.5 Hz, 2H), 7.62 (dd, J = 8.3, 1.2 Hz, 2H), 7.65 (dd, J = 7.5, 1.3 Hz, 1H), 7.76 (d, J = 2.0 Hz, 1H), 7.82−7.88 (m, 5H), 7.27 (bs, NH), 8.77 (d, J = 8.3 Hz, 1H), 8.87 (d, J = 1.7 Hz, 1H). ^{13}C{^{1}H} NMR (150.8 MHz, $CDCl_3$, 77.36 ppm, +25 °C): δ 22.9 (CH3), 122.1 (CH), 122.6 (CH), 124.4 (Cq), 124.6 (CH), 125.4 (CH), 126.6 (CH), 127.20 (CH), 127.22 (CH), 127.9 (CH), 128.1 (CH), 128.2 (CH), 128.5 (CH), 128.6 (CH), 128.8 (CH), 129.0 (CH), 129.4 (CH), 129.7 (CH), 131.5 (Cq), 131.6 (CH), 132.6 (Cq), 133.1 (bs, Cq), 134.4 (Cq), 135.6 (Cq), 136.6 (CH), 137.0 (bs, Cq), 138.45 (Cq), 138.48 (Cq), 139.0 (Cq), 141.2 (Cq). ^{11}B NMR (192.4 MHz, $CDCl_3$, BF_3·Et_2O = 0 ppm, +25 °C): δ 39.40. HRMS (ESI-QTOF): calcd for $C_{35}H_{27}BN$ $[M + H]^+$ 472.2231, found 472.2228. Semipreparative CSP-HPLC resolution was obtained with Chiralpak-AD-H column (250 × 21.2 mm, *n*-hexane/2-propanol 97:3 v/v, 20 mL/min).

1-Bromo-2-(propan-2-yloxy)naphthalene (4, CAS: 791088-70-5).[25] 1-Bromo-2-naphthol (2.23 g, 10 mmol) was dissolved in DMSO (20 mL), and a solution of KOH (3 mL, 4 M, 12 mmol) was added. The reaction was stirred at room temperature for about 15 min. Once the anion was formed, perceptible by a change of color, 2-iodopropane (2 mL, 20 mmol) was added. The reaction was allowed to stir for 2 h and monitored by TLC. The reaction was quenched with cold water and extracted with EtOAc (50 mL × 3). The combined organic phase was dried over of magnesium sulfate and solvent removed in vacuum. The crude product was purified with a silica chromatographic column (petroleum ether/DCM, 9:1). Yield = 97%, 2.57 g. ^{1}H NMR (600 MHz, $CDCl_3$, TMS, +25 °C): δ 1.36 (d, J = 6.1 Hz, 6H), 4.59 (q, J = 6.1 Hz, 1H), 7.14 (d, J = 8.9 Hz, 1H), 7.33 (t J = 7.5 Hz, 1H), 7.50 (t J = 7.6 Hz, 1H), 7.67 (d J = 8.9 Hz, 1H), 7.70 (d, J = 8.3 Hz, 1H), 8.21 (d, J = 8.5 Hz, 1H). ^{13}C{^{1}H} NMR (150.8 MHz, $CDCl_3$, 77.36 ppm, +25 °C): δ 22.7 ($2CH_3$), 73.6 (CH), 111.7 (Cq), 117.9 (CH), 124.7 (CH), 124.7 (CH), 126.7 (CH), 127.7 (CH), 128.2 (CH), 128.9 (CH), 130.4 (Cq), 133.6 (Cq), 152.9 (Cq). HRMS (ESI-QTOF): calcd for $C_{13}H_{14}OBr$ $[M + H]^+$ 265.0223, found 265.0227

■ ASSOCIATED CONTENT

Supporting Information

The Supporting Information is available free of charge on the ACS Publications website at DOI: 10.1021/acs.joc.9b01550.

Figures S1−S9, UV and ECD spectra of **3**, ^{1}H, ^{13}C, DEPT of **1a−1d** and **4**, ^{11}B spectra of **1a−1d**, and computational details for **1a−1d** and **3** (PDF).

■ AUTHOR INFORMATION

Corresponding Author

*E-mail: michele.mancinelli@unibo.it.

ORCID

Andrea Mazzanti: 0000-0003-1819-8863

Michele Mancinelli: 0000-0002-8499-5265

Notes

The authors declare no competing financial interest.

■ ACKNOWLEDGMENTS

A.M., E.M., and M.M. thank the University of Bologna (RFO funds 2017 and 2018). We thank Dr. Alessia Ciogli, University of Rome "La Sapienza" for the simulation of the D-HPLC spectra. ALCHEMY Fine Chemicals & Research (Bologna, www.alchemy.it) is acknowledged for a gift of chemicals.

■ REFERENCES

(1) (a) Giustra, Z. X.; Liu, S.-Y. The State of the Art in Azaborine Chemistry: New Synthetic Methods and Applications. *J. Am. Chem. Soc.* **2018**, *140*, 1184−1194. (b) Campbell, P. G.; Marwitz, A. J. V.; Liu, S.-Y. Recent Advances in Azaborine Chemistry. *Angew. Chem., Int. Ed.* **2012**, *51*, 6074−6092.

(2) Bosdet, M. J. D.; Jaska, C. A.; Piers, W. E.; Sorensen, T. S.; Parvez, M. Blue Fluorescent 4a-Aza-4b-boraphenanthrenes. *Org. Lett.* **2007**, *9*, 1395−1398.

DOI: 10.1021/acs.joc.9b01550
J. Org. Chem. 2019, 84, 12253−12258

(3) Wang, X.-Y.; Lin, H.-R.; Lei, T.; Yang, D.-C.; Zhuang, F.-D.; Wang, J.-Y.; Yuan, S.-C.; Pei, J. Azaborine Compounds for Organic Field-Effect Transistors: Efficient Synthesis, Remarkable Stability, and BN Dipole Interactions. *Angew. Chem., Int. Ed.* **2013**, *52*, 3117−3120.
(4) (a) Zhao, P.; Nettleton, D. O.; Karki, R. G.; Zécri, F. J.; Liu, S.-Y. Medicinal Chemistry Profiling of Monocyclic 1,2-Azaborines. *ChemMedChem* **2017**, *12*, 358−361. (b) Lee, H.; Fischer, M.; Shoichet, B. K.; Liu, S.-Y. Hydrogen Bonding of 1,2-Azaborines in the Binding Cavity of T4 Lysozyme Mutants: Structures and Thermodynamics. *J. Am. Chem. Soc.* **2016**, *138*, 12021−12024.
(5) Mazzanti, A.; Mercanti, E.; Mancinelli, M. Axial Chirality about Boron−Carbon Bond: Atropisomeric Azaborines. *Org. Lett.* **2016**, *18*, 2692−2695.
(6) (a) Christie, G. H.; Kenner, J. The Molecular Configurations of Polynuclear Aromatic Compounds. Part I. The Resolution of γ-6:6'-Dinitro- and 4:6:4':6'-Tetranitro-diphenic Acids into Optically Active Components. *J. Chem. Soc., Trans.* **1922**, *121*, 614−620. (b) Mazzanti, A.; Lunazzi, L.; Minzoni, M.; Anderson, J. E. Rotation in Biphenyls with a Single *ortho*-Substituent. *J. Org. Chem.* **2006**, *71*, 5474−5481.
(7) (a) Lunazzi, L.; Mancinelli, M.; Mazzanti, A.; Lepri, S.; Ruzziconi, R.; Schlosser, M. Rotational Barriers of Biphenyls Having Heavy Heteroatoms as *ortho*-Substituents: Experimental and Theoretical Determination of Steric Effects. *Org. Biomol. Chem.* **2012**, *10*, 1847−1855.
(8) (a) Lee, C.; Yang, W.; Parr, R. G. Development of the Colle-Salvetti Correlation-energy Formula into a Functional of the Electron Density. *Phys. Rev. B: Condens. Matter Mater. Phys.* **1988**, *37*, 785−789. (b) Becke, A. D. Density-functional Thermochemistry. III. The Role of Exact Exchange. *J. Chem. Phys.* **1993**, *98*, 5648−5652. (c) Stephens, P. J.; Devlin, F. J.; Chabalowski, C. F.; Frisch, J. M. Ab Initio Calculation of Vibrational Absorption and Circular Dichroism Spectra Using Density Functional Force Fields. *J. Phys. Chem.* **1994**, *98*, 11623−11627.
(9) Fingerle, M.; Maichle-Mössmer, C.; Schundelmeier, S.; Speiser, B.; Bettinger, H. F. Synthesis and Characterization of a Boron−Nitrogen−Boron Zigzag-Edged Benzo[fg]tetracene Motif. *Org. Lett.* **2017**, *19*, 4428−4431.
(10) Dewar, M. J. S.; Kubba, V. P.; Pettit, R. 624. New Heteroaromatic Compounds. Part I. 9-Aza-10-boraphenanthrene. *J. Chem. Soc.* **1958**, 3073−3076.
(11) Casarini, D.; Lunazzi, L.; Mazzanti, A. Recent Advances in Stereodynamics and Conformational Analysis by Dynamic NMR and Theoretical Calculations. *Eur. J. Org. Chem.* **2010**, *2010*, 2035−2056.
(12) (a) D'Acquarica, I.; Gasparrini, F.; Pierini, M.; Villani, C.; Zappia, G. Dynamic HPLC on Chiral Stationary Phases: A Powerful Tool for The Investigation of Stereomutation Processes. *J. Sep. Sci.* **2006**, *29*, 1508−1516. (b) Sabia, R.; Ciogli, A.; Pierini, M.; Gasparrini, F.; Villani, C. Dynamic High Performance Liquid Chromatography on Chiral Stationary Phases. Low Temperature Separation of the Interconverting Enantiomers of Diazepam, Flunitrazepam, Prazepam and Tetrazepam. *J. Chrom. A* **2014**, *1363*, 144−149. (c) Wolf, C.; Tumambac, G. E. Investigation of the Stereodynamics of Axially Chiral 1,8-Bis(2,2'-diphenyl-4,4'-dipyridyl)-naphthalene and Cryogenic Separation of Its *syn/anti*-Isomers. *J. Phys. Chem. A* **2003**, *107*, 815−817. (d) Wolf, C.; Hochmuth, D. H.; König, W. A.; Roussel, C. Influence of Substituents on the Rotational Energy Barrier of Axially Chiral Biphenyls, II. *Liebigs Ann. Chem.* **1996**, *1996*, 357−363. (e) Wolf, C.; König, W. A.; Roussel, C. Influence of Substituents on the Rotational Energy Barrier of Atropisomeric Biphenyls − Studies by Polarimetry and Dynamic Gas Chromatography. *Liebigs Ann. Chem.* **1995**, 781−786. See also: Wolf, C. *Dynamic Stereochemistry of Chiral Compounds, Principles and Applications*; RSC Publishing, 2008; Chapter 4.3, pp 153−164.
(13) Cirilli, R.; Costi, R.; Di Santo, R.; La Torre, F.; Pierini, M.; Siani, G. Perturbing Effects of Chiral Stationary Phase on Enantiomerization Second-Order Rate Constants Determined by Enantioselective Dynamic High-Performance Liquid Chromatography: A Practical Tool to Quantify the Accessible Acid and Basic Catalytic Sites Bonded on Chromatographic Supports. *Anal. Chem.* **2009**, *81*, 3560−3570.
(14) Ōki, M. *Recent Advances in Atropisomerism*; Allinger, N. L., Eliel, E. L., Wilen, S. H., Eds.; John Wiley & Sons: Hoboken, NJ, 1983; Topics in Stereochemistry Vol. *14*, pp 1−82.
(15) (a) Superchi, S.; Scafato, P.; Górecki, M.; Pescitelli, G. Absolute Configuration Determination by Quantum Mechanical Calculation of Chiroptical Spectra: Basics and Applications to Fungal Metabolites. *Curr. Med. Chem.* **2018**, *25*, 287−320. (b) Pescitelli, G.; Bruhn, T. Good Computational Practice in the Assignment of Absolute Configurations by TDDFT Calculations of ECD Spectra. *Chirality* **2016**, *28*, 466−474. (c) Laurent, A. D.; Jacquemin, D. TD-DFT benchmarks: A Review. *Int. J. Quantum Chem.* **2013**, *113*, 2019−2039. (d) Jacquemin, D.; Wathelet, V.; Perpète, E. A.; Adamo, C. Extensive TD-DFT Benchmark: Singlet-Excited States of Organic Molecules. *J. Chem. Theory Comput.* **2009**, *5*, 2420−2435.
(16) Yanai, T.; Tew, D.; Handy, N. A new Hybrid Exchange−correlation Functional Using the Coulomb-attenuating Method (CAM-B3LYP). *Chem. Phys. Lett.* **2004**, *393*, 51−57.
(17) (a) Chai, J.-D.; Head-Gordon, M. Long-range Corrected Hybrid Density Functionals with Damped Atom−atom Dispersion Corrections. *Phys. Chem. Chem. Phys.* **2008**, *10*, 6615−6620. (b) Iikura, H.; Tsuneda, T.; Yanai, T.; Hirao, K. A Long-range Correction Scheme for Generalized-gradient-approximation Exchange Functionals. *J. Chem. Phys.* **2001**, *115*, 3540−3544.
(18) In Gaussian 16 the BH&HLYP functional has the form: $0.5*^{EXHF} + 0.5*^{EXLSDA} + 0.5*\Delta EX^{Becke88} + EC^{LYP}$.
(19) Zhao, Y.; Truhlar, D. G. The M06 Suite of Density Functionals for Main Group Thermochemistry, Thermochemical Kinetics, Noncovalent Interactions, Excited States, and Transition Elements: Two New Functionals and Systematic Testing of Four M06-class Functionals and 12 other Functionals. *Theor. Chem. Acc.* **2008**, *120*, 215−241.
(20) Gunasekaran, P.; Perumal, S.; Menéndez, J. C.; Mancinelli, M.; Ranieri, S.; Mazzanti, A. Axial Chirality of 4-Arylpyrazolo[3,4-b]pyridines. Conformational Analysis and Absolute Configuration. *J. Org. Chem.* **2014**, *79*, 11039−11050.
(21) Brown, J. H.; Bushweller, C. H. *QCPE Bulletin*; QCPE: Bloomington, IN, 1983; Vol. *3*, pp 102−103. A copy of the program is available upon request from the authors (A.M. and M.M).
(22) *Gaussian 16*, rev A.03: Frisch, M. J.; Trucks, G. W.; Schlegel, H. B.; Scuseria, G. E.; Robb, M. A.; Cheeseman, J. R.; Scalmani, G.; Barone, V.; Mennucci, B.; Petersson, G. A.; Nakatsuji, H.; Caricato, M.; Li, X.; Hratchian, H. P.; Izmaylov, A. F.; Bloino, J.; Zheng, G.; Sonnenberg, J. L.; Hada, M.; Ehara, M.; Toyota, K.; Fukuda, R.; Hasegawa, J.; Ishida, M.; Nakajima, T.; Honda, Y.; Kitao, O.; Nakai, H.; Vreven, T.; Montgomery, J. A., Jr.; Peralta, J. E.; Ogliaro, F.; Bearpark, M.; Heyd, J. J.; Brothers, E.; Kudin, K. N.; Staroverov, V. N.; Kobayashi, R.; Normand, J.; Raghavachari, K.; Rendell, A.; Burant, J. C.; Iyengar, S. S.; Tomasi, J.; Cossi, M.; Rega, N.; Millam, N. J.; Klene, M.; Knox, J. E.; Cross, J. B.; Bakken, V.; Adamo, C.; Jaramillo, J.; Gomperts, R.; Stratmann, R. E.; Yazyev, O.; Austin, A. J.; Cammi, R.; Pomelli, C.; Ochterski, J. W.; Martin, R. L.; Morokuma, K.; Zakrzewski, V. G.; Voth, G. A.; Salvador, P.; Dannenberg, J. J.; Dapprich, S.; Daniels, A. D.; Farkas, O.; Foresman, J. B.; Ortiz, J. V.; Cioslowski, J.; Fox, D. J. Gaussian, Inc., Wallingford, CT, 2009.
(23) *GaussView 6.0.16*; Dennington, R. D., II, Keith, T. A., Millam, J. M.; Semichem, Inc., 2000−2016.
(24) Schaarschmidt, D.; Grumbt, M.; Hildebrandt, A.; Lang, H. A Planar-Chiral Phosphino(alkenyl)ferrocene for Suzuki−Miyaura C−C Coupling Reactions. *Eur. J. Org. Chem.* **2014**, *2014*, 6676−6685.
(25) Reddy, K. R.; Rajanna, K. C.; Uppalaiah, K.; Ramgopal, S. Cetyltrimethylammonium Bromide as an Efficient Catalyst for Regioselective Bromination of Alkoxy Naphthalenes with Trimethyl Benzyl Ammonium Tribromide: Synthetic and Kinetic Approach. *Int. J. Chem. Kinet.* **2014**, *46*, 10−15.

DOI: 10.1021/acs.joc.9b01550
J. Org. Chem. 2019, 84, 12253−12258